

Arnoldi methods for image deblurring with anti-reflective boundary conditions

Marco Donatelli*

David Martin†

Lothar Reichel‡

Abstract

Image deblurring with anti-reflective boundary conditions and a non-symmetric point spread function is considered. Several iterative methods based on Krylov subspace projections, as well as Arnoldi-Tikhonov regularization methods, with reblurring right or left preconditioners are compared. The aim of the preconditioner is not to accelerate the convergence, but to improve the quality of the computed solution and to increase the robustness of the regularization method. Right preconditioning in conjunction with methods based on the Arnoldi process are found to be robust and give high-quality restorations. In particular, when the observed image is contaminated by motion blur, our new method is much more effective than other approaches described in the literature, such as range restricted Arnoldi methods and the conjugate gradient method applied to the normal equations (implemented with the reblurring approach).

1 Introduction

We consider the restoration of blurred and noise-corrupted images, where the blurring is modeled by a convolution. In two space-dimensions this problem can be formulated as an integral equation of the form

$$g(\mathbf{x}) = [Kf](\mathbf{x}) + \nu(\mathbf{x}) = \int_{\mathbb{R}^2} h(\mathbf{x} - \mathbf{y}) f(\mathbf{y}) d\mathbf{y} + \nu(\mathbf{x}), \quad \mathbf{x} \in \Omega \subset \mathbb{R}^2, \quad (1)$$

where f represents the (unavailable) true image, h the space invariant point-spread function (PSF) with compact support, ν random noise, and g the (available) blurred and noise-corrupted image. Thus, f and g are real-values nonnegative functions that yield the gray-scale values of the images; see, e.g., [3] for a discussion of this model.

Discretization of the above integral equation at equidistant nodes yields

$$g_i = \sum_{j \in \mathbb{Z}^2} h_{i-j} f_j + \nu_i, \quad i \in \mathbb{Z}^2, \quad (2)$$

*Dipartimento di Scienza e Alta Tecnologia, Università dell’Insubria, Como 22100, Italy. E-mail: marco.donatelli@uninsubria.it

†Department of Mathematical Sciences, Kent State University, Kent, OH 44242, USA. E-mail: dmarti49@kent.edu

‡Department of Mathematical Sciences, Kent State University, Kent, OH 44242, USA. E-mail: reichel@math.kent.edu

where the entries of the discrete images $\mathbf{g} = [g_i]$ and $\mathbf{f} = [f_j]$ represent the light intensity at each pixel and $\boldsymbol{\nu} = [\nu_i]$ models the noise-contamination at these pixels.

We are interested in determining an accurate approximation of the true image \mathbf{f} in the finite field of view (FOV) corresponding to $i \in [1, n]^2$, given $\mathbf{h} = [h_i]$, distributional information about $\boldsymbol{\nu}$, and the blurred image \mathbf{g} in the same FOV. The FOV is assumed to be square only for notational simplicity.

The linear system of equations defined by (2) with i restricted to $[1, n]^2$ is underdetermined when there are nonvanishing coefficients h_i with $i \neq 0$, since then there are n^2 constraints, while the number of unknowns required to specify the equations is larger. A meaningful solution of this system can be determined in several ways. For instance, one may determine the solution of minimal Euclidean norm of the underdetermined system; see [4, 28] for discussions of this approach. Alternatively, one can determine a linear system of equations with a square matrix,

$$A\mathbf{f} = \mathbf{g}, \quad A \in \mathbb{R}^{n^2 \times n^2}, \quad \mathbf{f}, \mathbf{g} \in \mathbb{R}^{n^2}, \quad (3)$$

by imposing boundary conditions (BC), where the f_j -values in (2) at pixels outside the FOV are assumed to be certain linear combinations of values inside the FOV. Popular boundary conditions include zero Dirichlet boundary conditions (ZDBC), periodic boundary conditions (PBC), reflective boundary conditions (RBC) discussed in [23], and anti-reflective boundary conditions (ARBC) proposed in [27]. An illustration of images that satisfy these boundary conditions can be found in, e.g., [18]. Further details can be found in Section 2.

We say that an image \mathbf{f} is discontinuous at the boundary, if the corresponding continuous function f has to have a discontinuity or a steep gradient in order for \mathbf{f} to be a discretization of f .¹ For generic images, both ZDBC and PBC usually introduce discontinuities in the image \mathbf{g} at the boundary, often resulting in artifacts such as “ringing” near the boundary of the restored image \mathbf{f} . Generally, such artifacts can be reduced significantly by the use of RBC or ARBC, since both these boundary conditions impose continuity of the extended image at the boundary. Further, ARBC tend to reduce artifacts near the boundary of the restored image \mathbf{f} more than RBC, because the former boundary conditions also impose continuity of the normal derivative of the extended image at the boundary. Similarly as continuity, the notion of a normal derivative has to be suitably interpreted.

When the PSF h is quadrantly symmetric, i.e., when

$$h(x_1, x_2) = h(|x_1|, |x_2|) \quad \forall \mathbf{x} = [x_1, x_2]^T \in \Omega,$$

such as the PSF associated with symmetric Gaussian blur, there are fast transforms for diagonalizing the matrix A in (3) when RBC or ARBC are imposed. These transforms can be applied to devise fast filtering methods for the approximate solution of (3); see [1, 8, 23]. For many more general PSFs of interest in applications, fast filtering methods are not available. For instance, let the matrix A be determined by a nonsymmetric PSF h that models motion blur with RBC or ARBC. Then there are fast algorithms for the evaluation of matrix-vector products with A , but there is no known direct algorithm for the fast approximate solution of the associated linear system of equations (3). Therefore, when using RBC or ARBC with this kind of PSF, one generally resorts to iterative methods for the restoration of large images.

¹We may, for instance, consider f to be a piecewise linear function that interpolates the pixel values \mathbf{f} .

The adjoint of the convolution operator in (1) is the correlation operator

$$[K^* f](\mathbf{x}) = \int_{\mathbb{R}^2} h(\mathbf{y} - \mathbf{x}) f(\mathbf{y}) d\mathbf{y}, \quad (4)$$

where we have used the fact that h is real-valued. In [9], the authors propose to replace the system (3) by

$$A' A \mathbf{f} = A' \mathbf{g} \quad (5)$$

when RBC or ARBC are imposed and the PSF is quite general. The matrix A' is obtained from the discretization of (4) with the same boundary conditions as for (3), i.e., from the PSF rotated 180°. The system (5) offers an alternative to the normal equations,

$$A^T A \mathbf{f} = A^T \mathbf{g}, \quad (6)$$

when the evaluation of matrix-vector products with the transpose A^T of the matrix A is complicated or time-consuming. This situation arises when the matrix A is not explicitly stored and has a structure that can be utilized when evaluating matrix-vector products efficiently, while the structure of A^T is more difficult to exploit. This is the case, for instance, when A is defined by a convolution in two or more space-dimension and ARBC are imposed. We remark that in one space-dimension, matrix-vector products with A and A^T can be evaluated about equally rapidly. Further comments on the difficulties of using A^T are provided in Section 2.

The solution of (5) has been shown to reduce boundary artifacts when the PSF is a symmetric convolution; see [11] and Section 5 for illustrations that compare restorations determined by solving (5) and (6), as well as the unpreconditioned system (3). The solution of (5) is found to give the best restorations. Note that when either ZDBC or PBC are imposed, we have $A' = A^T$ and, hence, the equation (5) agrees with the normal equations (6).

The standard CGLS method is an efficient implementation of the conjugate gradient method applied to the normal equations (6). The method applies a three-term recursion, which is analogous to the one used by the symmetric Lanczos process, to reduce a large symmetric matrix to a small symmetric tridiagonal matrix; see [5] for details. In [9], the recursion formulas for CGLS are applied to the solution of (5) when ARBC are imposed. Thus, the iterative method for the solution of (5) is obtained by simply replacing the matrix A^T by A' in the recursion formulas for CGLS. This iterative method yields satisfactory numerical results for some problems. However, an obvious flaw of this method is that since $A' A$ is not symmetric, the use of the three-term recurrence relation of the Lanczos process is not justified. The satisfactory performance of the algorithm reported in [9] can be explained by the fact that the anti-symmetric part of $A' A$, given by

$$\frac{1}{2} \left(A' A - (A' A)^T \right),$$

is of much smaller norm than the symmetric part, and is of rank of at most order n . However, the lack of theoretical justification for the use of CGLS in this context makes it natural to explore the performance of other iterative methods. Moreover, this theoretical flaw leads to inaccurate restorations when the observed image is contaminated by motion blur, cf. Examples 3 and 4 in Section 5.

It is the purpose of the present paper to compare the performance of several iterative methods when they are applied to the solution of linear systems of equations (5) with a matrix A determined by a convolution that is not quadrantly symmetric and by ARBC. We may consider (5) a left-preconditioned versions of (3). Also the right-preconditioned version,

$$AA'z = g, \quad (7)$$

whose solution z yields the approximate solution $f = A'z$ of (3), will be considered. The system (7) has not previously been discussed in the literature. It has the advantage over (5) that its residual is well suited for use with the discrepancy principle to decide how many iterations to carry out; see below. When the matrix A is large, the computational cost of one iteration with the Arnoldi method applied to (7) is almost the same as the cost of one iteration of CGLS applied to (5). However, the numerical results in Section 5 show that the former method is more robust and effective for several different kinds of blur and noise levels than the latter.

We discuss the iterative solution of the linear systems of equations (3), (5), and (7) by the standard GMRES method by Saad and Schultz [26], by the range restricted GMRES (RRGMRES) method described in [22], and compare with the approximate solutions of (5) computed by the CGLS method. Regularization is achieved by early termination of the iterations.

Tikhonov regularization is an alternative to regularization by early termination. This regularization method replaces the linear systems of equations (3), (5), or (7) by penalized least-squares problems. We discuss the performance of Tikhonov regularization when the solution of the minimization problem is restricted to the same kind of Krylov subspaces as the solution of the standard GMRES method when applied to the solution of (3), (5), and (7). This Tikhonov regularization method is described in [7]; see also [16, 17] for recent discussions. Moreover, we consider Tikhonov regularization when the solution is restricted to the same kind of Krylov subspaces as the solution of the RRGMRES method; see [19, 20, 22] for discussions on the implementation and performance of the latter methods.

This paper is organized as follows. In Section 2 we give a brief overview of anti-reflective boundary conditions. Section 3 describes the iterative methods that we are considering, including the Tikhonov regularization methods mentioned above, and Section 4 discusses the benefits of solving preconditioned systems. Section 5 presents numerical examples that illustrate the performance of the methods discussed, and Section 6 contains concluding remarks.

2 Anti-reflective boundary conditions

This section recalls some properties of blurring matrices obtained with ARBC. We begin with problems in one space-dimension and then proceed to two space-dimensions. A survey of this topic is provided in [12].

2.1 The 1D case

In deblurring problems in one space-dimension, the matrix of the underdetermined linear system associated to (2) is of the form

$$\tilde{A} = \begin{pmatrix} h_m & \cdots & h_0 & \cdots & h_{-m} & & 0 \\ & h_m & & h_0 & & h_{-m} & \\ & & \ddots & \ddots & \ddots & \ddots & \\ & & & \ddots & \ddots & \ddots & \\ & & & & h_m & h_0 & h_{-m} \\ 0 & & & & h_m & \cdots & h_0 & \cdots & h_{-m} \end{pmatrix} \in \mathbb{R}^{n \times (n+2m)},$$

where typically $1 < m \ll n$. Thus, the blurred signal $\mathbf{g} = [g_1, g_2, \dots, g_n]^T$ is determined not only by the entries of $\mathbf{f} = [f_1, f_2, \dots, f_n]^T$, but also by f_{-m+1}, \dots, f_0 and f_{n+1}, \dots, f_{n+m} . To remove the dependency of \mathbf{g} on the unknown boundary data f_{-m+1}, \dots, f_0 and f_{n+1}, \dots, f_{n+m} , we make certain assumptions (referred to as boundary conditions) about the unknown boundary data so that the number of unknowns equals the number of equations. ARBC are defined by assuming that the data outside the FOV are anti-reflections of the data inside. More precisely, we require that

$$\begin{aligned} f_{1-j} &= f_1 - (f_{j+1} - f_1) = 2f_1 - f_{j+1}, \\ f_{n+j} &= f_n - (f_{n-j} - f_n) = 2f_n - f_{n-j}, \end{aligned} \quad j = 1, 2, \dots, m. \quad (8)$$

Define the vectors $\mathbf{u} = [u_j], \mathbf{w} = [w_j] \in \mathbb{R}^n$ with the nontrivial components

$$u_j = 2 \sum_{k=j}^m h_k, \quad w_{n+1-j} = 2 \sum_{k=j}^m h_{-k}, \quad 1 \leq j \leq m,$$

and the remaining components zero. Thus, $u_{m+1} = \dots = u_n = 0$ and $w_1 = \dots = w_{n-m} = 0$. The resulting $n \times n$ blurring matrix A in (3), with n^2 replaced by n , is given by

$$A = \mathbf{u}\mathbf{e}_1^T - L + T - R + \mathbf{w}\mathbf{e}_n^T, \quad (9)$$

where $\mathbf{e}_k = [0, \dots, 0, 1, 0, \dots, 0]^T$ is the k th vector of the canonical basis and the matrices L , T , and R are given by

$$\left(\begin{array}{cccc} 0 & h_1 & \cdots & h_m \\ \vdots & \vdots & \ddots & \\ & h_m & & 0 \\ \vdots & & & \\ 0 & & & \end{array} \right), \left(\begin{array}{ccccc} h_0 & \cdots & h_{-m} & & 0 \\ \vdots & \ddots & \ddots & \ddots & \\ h_m & \ddots & \ddots & \ddots & h_{-m} \\ & \ddots & \ddots & \ddots & \vdots \\ 0 & & h_m & \cdots & h_0 \end{array} \right), \left(\begin{array}{ccccc} & & & & 0 \\ & & & & \vdots \\ & & & & h_{-m} \\ & & & \ddots & \vdots \\ h_{-m} & \cdots & h_{-1} & 0 & \end{array} \right),$$

respectively; see [27] for details. The matrices $L \in \mathbb{R}^{n \times n}$ and $R \in \mathbb{R}^{n \times n}$ have nonvanishing entries only in the leading and trailing principal submatrices of order $m+1$, respectively. Except for

their first or last columns, these submatrices are of Hankel-type. The first and last columns are modified by rank-one matrices in (9). Hence, the matrix A in (9) is Toeplitz plus Hankel plus a rank-2 matrix. Therefore, matrix-vector products with A can be computed efficiently by application of the fast Fourier transform (FFT). A simple way to implement the matrix-vector product evaluation is to use an anti-symmetric pad (padding according to (8) in every direction), and then apply a circulant convolution by using the FFT, and selecting only elements of the result that are in the FOV.² Note that the matrix A in (9) is not symmetric, also in the case of a symmetric PSF, due to the rank-2 component.

Consider a symmetric PSF. Then $h_j = h_{-j}$ for all j . Let $Q = [q_{i,j}]$ be the type I sine transform matrix of order $n - 2$ with entries

$$q_{i,j} = \sqrt{\frac{2}{n-1}} \sin\left(\frac{j i \pi}{n-1}\right), \quad i, j = 1, 2, \dots, n-2.$$

Then Q is real, orthogonal, and symmetric, i.e., $Q^{-1} = Q^T = Q$. We define the anti-reflective transform by

$$S_n = \begin{bmatrix} \mathbf{1} & \mathbf{0} \\ Q & \mathbf{0} \\ \mathbf{0} & \boldsymbol{\ell} \end{bmatrix}, \quad (10)$$

where

$$\mathbf{1} = \frac{1}{\sqrt{n}} \begin{bmatrix} 1 \\ 1 \\ \vdots \\ 1 \\ 1 \end{bmatrix} \quad \text{and} \quad \boldsymbol{\ell} = [\ell_i] = \frac{\sqrt{3}}{\sqrt{n(n^2-1)}} \begin{bmatrix} 1-n \\ 3-n \\ \vdots \\ n-3 \\ n-1 \end{bmatrix}.$$

Thus,

$$\begin{aligned} \ell_i &= \frac{\sqrt{3}}{\sqrt{n(n^2-1)}}(2i-1-n), & i &= 1, 2, \dots, \lfloor \frac{n+1}{2} \rfloor, \\ \ell_{n+1-i} &= -\ell_i, & i &= 1, 2, \dots, \lfloor \frac{n}{2} \rfloor, \end{aligned}$$

where $\lfloor \alpha \rfloor$ denotes the integer part of $\alpha \geq 0$.

The vectors $\mathbf{1}$ and $\boldsymbol{\ell}$ form an orthonormal basis for the grid samples of all linear polynomials. The spectral decomposition of A can now be written as

$$A = S_n \Lambda_n S_n^{-1}, \quad (11)$$

where

$$\Lambda_n = \text{diag}[\lambda_1, \lambda_2, \dots, \lambda_n]$$

with

$$\lambda_j = \begin{cases} \theta\left(\frac{j-1}{n-1}\pi\right), & 1 \leq j < n, \\ \theta(0), & j = n, \end{cases}$$

²A version of the MATLAB `padarray` function, that also contains the anti-symmetric pad for d -dimensional arrays can be downloaded from <http://scienze-como.uninsubria.it/mdonatelli/Software/software.html>.

and

$$\theta(x) = \sum_{j=-m}^m h_j e^{ijx}, \quad i = \sqrt{-1}. \quad (12)$$

Since the PSF averages nearby pixels, $h_j \geq 0$ for all j , and $\theta(0) = \sum_{j=-m}^m h_j = 1$, linear polynomials are perfectly reconstructed; see [1] for details.

The spectral decomposition (11) is useful for analyzing solution methods for the systems (5) and (7), since $A' = A$ for symmetric PSFs. In this situation all eigenvalues of A^2 are real and nonnegative, because the symbol (12) simplifies to a cosine polynomial and the eigenvalues of A are real. This reblurring strategy was proposed in [11], where numerical tests showed that the use of the matrix A^T in the case of ARBC can give rise to artifacts close to the boundary. These artifacts are caused by the fact that the entries of the first and last rows of A^T sum to values larger than one. Therefore, the inner product of these rows with a vector do not provide a convex combination of the entries of the vector. This observation lead the authors of [11] to suggest that A^T in (6) be replaced by the blurring matrix A . Subsequently, it was shown in [10] that this approach gives rise to a regularization method in a well-defined sense. Further discussions on the replacement of A^T in (6) by A are provided in [1, 8].

When the PSF is not symmetric, A^T should not be replaced by the blurring matrix A in (6). It was suggested in [9] that A^T instead be replaced by the matrix A' obtained by discretizing the correlation operator (4). An analysis of this replacement for classical BCs, such as ZDBC, PBC, and RBC is provided in [9].³ Unfortunately, $A'A$ is not symmetric for ARBC. Therefore the CGLS iterative method, which uses A^T and is based on the fact that $A^T A$ is symmetric and positive semi-definite, may yield poor restorations when A^T is replaced by A' ; see [15] and Section 5 for examples. Therefore, in the present paper, we consider iterative methods based on the Arnoldi process. These methods do not require the symmetry and positive semidefiniteness of $A'A$ or AA' , but may benefit from the presence of the matrix A' in the linear systems of equations (5) and (7).

2.2 The 2D case

The ARBC have a natural extension in two space-dimensions. Consider a blurring matrix determined by a discretized PSF, whose support is a square of $(2m+1) \times (2m+1)$ pixels with $2m+1 \leq n$ and central coefficient $h_{0,0}$. The image values $f_{1-j,t}$ for $1 \leq j \leq m$ and $1 \leq t \leq n$ are represented by $2f_{1,t} - f_{j+1,t}$. Analogously, for $1 \leq j \leq m$ and $1 \leq s, t \leq n$, we have

$$f_{s,1-j} = 2f_{s,1} - f_{s,j+1}, \quad f_{n+j,t} = 2f_{n,t} - f_{n-j,t}, \quad f_{s,n+j} = 2f_{s,n} - f_{s,n-j}.$$

When both indices are outside the range $\{1, 2, \dots, n\}$, which happens for pixels close to the four corners of the given image, we carry out anti-reflection first in one space-direction (in the direction of the x - or y -axis) and then in the other direction; see [13]. We describe these anti-reflections for pixels near the corner $(1, 1)$ of an image; pixels near the other corners are treated analogously. Thus, for $1 \leq j, l \leq m$, we let

$$f_{1-j,1-l} = 4f_{1,1} - 2f_{1,l+1} - 2f_{j+1,1} + f_{j+1,l+1}.$$

³We remark that $A' = A^T$ when zero Dirichlet or periodic boundary conditions are imposed.

Here we have carried out anti-reflection along the x -axis followed by anti-reflection along the y -axis.

The strategy to anti-reflect first in one space-direction and then in an orthogonal direction yields blurring matrices with a two-level structure associated with the structure obtained by reflection in one space-dimension; see [13]. Specifically, the matrix $A \in \mathbb{R}^{n^2 \times n^2}$ is the sum of five matrices: a block Toeplitz matrix with Toeplitz blocks, a block Toeplitz matrix with Hankel blocks, a block Hankel matrix with Toeplitz blocks, a block Hankel matrix with Hankel blocks, and a matrix of rank $4n$. Therefore, in two space-dimensions, the “low rank” correction (of rank $4n$) of the space invariant structures is not negligible and a standard linear algebra implementation of a matrix-vector product evaluation may require $O(n^3)$ arithmetic floating-point operations (flops). Nevertheless, by using the anti-symmetric pad followed by convolution, similarly as in the case of one space-dimension, matrix-vector product evaluations with A and A' can be implemented by applying two FFTs in only $\mathcal{O}(n^2 \log(n))$ flops. On the other hand, to the best of our knowledge, there is no simple implementation for the evaluation of matrix-vector products with A^T that requires $\mathcal{O}(n^2 \log(n))$ flops.

The computational cost of matrix-vector product evaluations is not the only shortcoming associated with the use of the matrix A^T , because as already observed in the 1D case, the replacement of A^T by A' in (6) was introduced in [11] with the aim of reducing possible artifacts close to the boundary.

Similarly as in the case of one space-dimension, a blurring matrix A associated with a quadrantly symmetric PSF can be diagonalized by the 2D anti-reflective transform

$$A = (S_n \otimes S_n) D_n (S_n \otimes S_n)^{-1},$$

where S_n is defined in (10), and the diagonal matrix D_n , whose nontrivial entries are the eigenvalues of A , is defined by a proper ordering of the uniform sampling of the bivariate symbol

$$\Theta(x, y) = \sum_{s=-m}^m \sum_{t=-m}^m h_{s,t} e^{i(sx+ty)}$$

at the grid points (x_i, y_j) for $i, j = 1, 2, \dots, n$, where $x_i = (i-1)\pi/(n-1)$ and $y_j = (j-1)\pi/(n-1)$ for $1 \leq i, j < n$, and $x_n = y_n = 0$; see [2] for a complete analysis of the spectrum of A .

The analysis in [10] shows the regularization properties to usually be very satisfactory for quadrantly symmetric PSFs, and so are the reported computed results. However, there is no satisfactory solution method for image restoration problems with a PSF that is far from quadrantly symmetric, such as a PSF that models motion blur, with ARBC. We show in this paper that these kind of restoration problems can be solved efficiently by combining iterative methods based on the Arnoldi process with the use of the matrix A' .

3 GMRES and Arnoldi–Tikhonov-type methods

This section describes the iterative methods that we will apply to the solution of equations (3), (5), and (7) when the matrices A and A' are determined by a nonsymmetric PSF and ARBC.

3.1 Iterative methods based on the standard Arnoldi process

We begin with a discussion of iterative solution methods that are based on the standard Arnoldi process. Specifically, we describe GMRES and Arnoldi–Tikhonov (AT) methods and discuss their application to the solution of a generic linear system of equations,

$$M\mathbf{x} = \mathbf{b}, \quad (13)$$

with a square matrix $M \in \mathbb{R}^{n \times n}$. The systems (3), (5), and (7) can be solved by letting $M = A$ and $\mathbf{b} = \mathbf{g}$, $M = A'A$ and $\mathbf{b} = A'\mathbf{g}$, and $M = AA'$ and $\mathbf{b} = \mathbf{g}$, respectively.

Assume that \mathbf{b} is corrupted by an error $\boldsymbol{\nu}$ of norm ε , and let \mathbf{b}_{true} denote the error-free vector associated with \mathbf{b} . Thus, $\mathbf{b} = \mathbf{b}_{\text{true}} + \boldsymbol{\nu}$. The vector \mathbf{b} represents available data, while \mathbf{b}_{true} is assumed not to be available. We will in the computed examples reported in Section 5 assume that an estimate of ε is known.

Given a linear system (13), $\ell \ll n$ steps of the Arnoldi process with initial vector $\mathbf{v}_1 = \mathbf{b}/\|\mathbf{b}\|$ yield the decomposition

$$MV_\ell = V_{\ell+1}H_{\ell+1,\ell}, \quad (14)$$

where $V_\ell = [\mathbf{v}_1, \dots, \mathbf{v}_\ell] \in \mathbb{R}^{n \times \ell}$ satisfies $V_\ell^T V_\ell = I$, and $H_{\ell+1,\ell} \in \mathbb{R}^{(\ell+1) \times \ell}$ is of upper Hessenberg form. Here I denotes the identity matrix and $\|\cdot\|$ stands for the Euclidean vector norm. The columns of V_ℓ form an orthonormal basis for the ℓ -dimensional Krylov subspace

$$\mathcal{K}_\ell(M, \mathbf{b}) = \text{span}\{\mathbf{b}, M\mathbf{b}, \dots, M^{\ell-1}\mathbf{b}\}. \quad (15)$$

We assume that ℓ is chosen small enough so the decomposition (14) with the stated properties exists. This is the generic situation.

GMRES determines an approximate solution of (13) by solving the minimization problem

$$\min_{\mathbf{x} \in \mathcal{K}_\ell(M, \mathbf{b})} \|M\mathbf{x} - \mathbf{b}\|, \quad (16)$$

whose solution is fairly easy to compute. Introduce the QR factorization

$$H_{\ell+1,\ell} = Q_{\ell+1,\ell+1}R_{\ell+1,\ell}, \quad (17)$$

where the matrix $Q_{\ell+1,\ell+1} \in \mathbb{R}^{(\ell+1) \times (\ell+1)}$ is orthogonal and $R_{\ell+1,\ell} \in \mathbb{R}^{(\ell+1) \times \ell}$ has a leading upper triangular submatrix $R_{\ell,\ell} \in \mathbb{R}^{\ell \times \ell}$ and a vanishing last row. It is worth mentioning that $Q_{\ell+1,\ell+1}$ can be represented as a product of ℓ Givens rotations. This makes it possible to update the factorization (17) when ℓ is increased by one in only $O(\ell)$ flops; see [26] for details. The assumptions on the decomposition (14) imply that the submatrix $R_{\ell,\ell}$ is invertible. Expressing $\mathbf{x} \in \mathcal{K}_\ell(M, \mathbf{b})$ as $\mathbf{x} = V_\ell \mathbf{y}$ and using the decompositions (14) and (17), and the fact that $\mathbf{v}_1 = \mathbf{b}/\|\mathbf{b}\|$, we obtain

$$\begin{aligned} \|M\mathbf{x} - \mathbf{b}\| &= \|MV_\ell \mathbf{y} - \mathbf{b}\| = \|V_{\ell+1}H_{\ell+1,\ell}\mathbf{y} - \mathbf{b}\| = \|H_{\ell+1,\ell}\mathbf{y} - \|\mathbf{b}\|\mathbf{e}_1\| \\ &= \|Q_{\ell+1,\ell+1}R_{\ell+1,\ell}\mathbf{y} - \|\mathbf{b}\|\mathbf{e}_1\| \\ &= \left\| \begin{bmatrix} R_{\ell,\ell} \\ \mathbf{0} \end{bmatrix} \mathbf{y} - \|\mathbf{b}\|Q_{\ell+1,\ell+1}^T \mathbf{e}_1 \right\|. \end{aligned}$$

Letting

$$\|\mathbf{b}\|Q_{\ell+1,\ell+1}^T \mathbf{e}_1 = \begin{bmatrix} \mathbf{q}_\ell \\ r_\ell \end{bmatrix}, \quad (18)$$

the solution \mathbf{x}_ℓ of (16) can be determined by first solving

$$R_{\ell,\ell} \mathbf{y} = \mathbf{q}_\ell$$

for \mathbf{y}_ℓ and then computing $\mathbf{x}_\ell = V_\ell \mathbf{y}_\ell$. The residual vector associated with (13) satisfies

$$\mathbf{r}_\ell = \mathbf{b} - M\mathbf{x}_\ell = \mathbf{g} - A\mathbf{x}_\ell \quad (19)$$

with

$$\|\mathbf{r}_\ell\| = |r_\ell|. \quad (20)$$

Let \mathbf{x}_{true} represent the exact solution of the linear system of equations $M\mathbf{x} = \mathbf{b}_{\text{true}}$, which is assumed to be consistent. We would like to determine an accurate approximation of \mathbf{x}_{true} by carrying out suitably many iterations with GMRES applied to (13). For the problems of interest, the matrix M is severely ill-conditioned and possibly singular; its singular values decay gradually to zero without a significant gap. The error $\|\mathbf{x}_\ell - \mathbf{x}_{\text{true}}\|$ of the GMRES iterates \mathbf{x}_ℓ generally decreases monotonically for the first few iterations, as an enlargement of the Krylov subspace (15) allows increasingly better approximations of \mathbf{x}_{true} , before reaching a minimum value and thereafter increases monotonically as the propagated error stemming from the error $\boldsymbol{\nu}$ in \mathbf{b} dominates the computed iterates \mathbf{x}_ℓ . This behavior of the iterates is typical for many iterative methods, including CGLS, when applied to the solution of linear systems of equations (13). It is therefore important that the iterations be terminated sufficiently early so that the error $\|\mathbf{x}_\ell - \mathbf{x}_{\text{true}}\|$ is close to minimal. The availability of an estimate ε of $\|\boldsymbol{\nu}\|$ allows us to terminate the iterations with the aid of the discrepancy principle. Thus, we accept the first iterate \mathbf{x}_ℓ such that

$$\|\mathbf{r}_\ell\| < \eta\varepsilon \quad (21)$$

as an approximation of \mathbf{x}_{true} ; see [6, 14] for justifications of this stopping criterion. Here $\eta \geq 1$ is a user-specified constant independent of ε . We comment on the choice of η in Section 5. Note that the norm $\|\mathbf{r}_\ell\|$ is available for free when the vector (18) has been computed; cf. (20).

When instead GMRES is applied to the solution of (5), the method determines iterates \mathbf{x}_ℓ with associated residual vectors

$$\mathbf{r}_\ell = \mathbf{b} - M\mathbf{x}_\ell = A'\mathbf{g} - A'A\mathbf{x}_\ell.$$

These residual vectors differ from the residual vectors (19) and cannot be used in the discrepancy principle. Therefore, the use of the discrepancy principle as stopping criterion for the iterations demand occasional evaluation of the norm of the residual error $\|\mathbf{b} - A\mathbf{x}_\ell\|$ to determine whether (21) holds. Each evaluation of the residual norm requires the computation of a matrix-vector product with A . We omit implementation details, because the iterates determined by GMRES when applied to (7) typically provide comparable or better approximations of \mathbf{x}_{true} than the iterates determined by GMRES when applied to (5); see Section 5 for illustrations. The former iterates, which we denote by \mathbf{z}_ℓ , define the approximate solution $\mathbf{x}_\ell = A'\mathbf{z}_\ell$ of (3) and yield

$$\mathbf{r}_\ell = \mathbf{b} - M\mathbf{x}_\ell = \mathbf{g} - AA'\mathbf{z}_\ell = \mathbf{g} - A\mathbf{x}_\ell.$$

It follows that the discrepancy principle can be applied in a straightforward manner when solving (7) by the GMRES method.

The Arnoldi–Tikhonov (AT) method replaces (16) by a penalized least-squares problem of the form

$$\min_{\mathbf{x} \in \mathcal{K}_\ell(M, \mathbf{b})} \{\|M\mathbf{x} - \mathbf{b}\|^2 + \mu\|L\mathbf{x}\|^2\} \quad (22)$$

with $L \in \mathbb{R}^{p \times n}$, where $p \geq 1$. We will let $L = I$ in this paper; however, extensions to more general matrices L can be developed; see, e.g., [24, 25] for discussions and references. The purpose of the regularization parameter $\mu > 0$ is to provide a suitable balance between the terms in (22). Its value should depend both on the problem being solved and on the amount of error in the data \mathbf{b} ; see below. The minimization problem (22) has a unique solution \mathbf{x}_μ for any $\mu > 0$.

Let V_ℓ be determined by (14) and let $\mathbf{x} = V_\ell \mathbf{y}$. Then the problem (22) with $L = I$ can be expressed as

$$\min_{\mathbf{y} \in \mathbb{R}^\ell} \{\|R_{\ell,\ell} \mathbf{y} - \mathbf{q}_\ell\|^2 + \mu\|\mathbf{y}\|^2\},$$

where \mathbf{q}_ℓ is defined by (18). This problem can be written as

$$\min_{\mathbf{y} \in \mathbb{R}^\ell} \left\| \begin{bmatrix} R_{\ell,\ell} \\ \sqrt{\mu} I_\ell \end{bmatrix} \mathbf{y} - \begin{bmatrix} \mathbf{q}_\ell \\ \mathbf{0} \end{bmatrix} \right\|. \quad (23)$$

The solution $\mathbf{y}_{\mu,\ell}$ can be computed by QR factorization of the matrix in (23), and the corresponding solution of (22) is given by $\mathbf{x}_{\mu,\ell} = V_\ell \mathbf{y}_{\mu,\ell}$.

We use the discrepancy principle to determine a suitable value of the regularization parameter $\mu > 0$. For a fixed value of ℓ , we seek to determine $\mu = \mu_{\ell,\varepsilon}$ such that $\mathbf{x}_{\mu,\ell} = V_\ell \mathbf{y}_{\mu,\ell}$, where $\mathbf{y}_{\mu,\ell}$ solves (23), satisfies

$$\|M\mathbf{x}_{\mu,\ell} - \mathbf{b}\| = \eta\varepsilon, \quad (24)$$

where $\eta \geq 1$ is the same constant as in (21).

Proposition 1 *Let $\mu > 0$ and let $\mathbf{x}_{\mu,\ell} = V_\ell \mathbf{y}_{\mu,\ell}$ be an approximation of \mathbf{x}_{true} determined by solving (23) for $\mathbf{y}_{\mu,\ell}$. Let \mathbf{x}_ℓ be determined by application of ℓ steps of GMRES to the solution of (13). Then*

$$\|M\mathbf{x}_{\mu,\ell} - \mathbf{b}\| > \|M\mathbf{x}_\ell - \mathbf{b}\|.$$

Proof. The result follows by comparing the minimization problems (16) and (22). \square

It follows from the above proposition that a necessary and sufficient condition for (24) to have a solution $\mathbf{x}_{\mu,\ell}$ with $0 < \mu < \infty$ is that ℓ be large enough so that (21) holds. The determination of μ such that (24) is satisfied is equivalent to the task of finding the largest zero of the function

$$\psi_\ell(\mu) := \|R_{\ell,\ell} \mathbf{y}_{\mu,\ell} - \mathbf{q}_\ell\|^2 - \eta^2 \varepsilon^2.$$

One can show, e.g., by using the singular value decomposition of $R_{\ell,\ell}$, that

$$\psi_\ell(\mu) = \mu^2 \mathbf{q}_\ell^T (R_{\ell,\ell} R_{\ell,\ell}^T + \mu I)^{-2} \mathbf{q}_\ell - \eta^2 \varepsilon^2.$$

The desired zero of ψ_ℓ can be conveniently computed by applying Newton's method to the function $\nu \rightarrow \psi_\ell(1/\nu)$; see, e.g., [19] for details. In particular, we note that when determining an

approximate solution of (3) or (7) by Tikhonov regularization with the regularization parameter $\mu = \mu_{\ell,\varepsilon}$ determined by the discrepancy principle, the value $\mu_{\ell,\varepsilon}$ can be computed efficiently for each fixed ℓ by working only with matrices of order ℓ .

Application of the discrepancy principle when solving (5) requires explicit computation of the norm of the residual error $\mathbf{r}_{\mu,\ell} = \mathbf{b} - A\mathbf{x}_{\mu,\ell}$, which, in turn, demands explicit computation of the approximate solution $\mathbf{x}_{\mu,\ell}$ and its multiplication by A . These computations have to be carried out several times for every value of ℓ . Clearly, the application of the discrepancy principle when solving (5) by Tikhonov regularization is more cumbersome than when determining approximate solutions of (3) and (7) in an analogous manner. We will not dwell on the details, because the computed solutions of (7) typically provides comparable or better approximations of \mathbf{x}_{true} than the corresponding solutions of (5). This is illustrated in Section 5.

3.2 Iterative methods based on the range restricted Arnoldi process

We consider iterative solution methods based on the range restricted Arnoldi process, in particular RRGMRES and the range restricted Arnoldi–Tikhonov (RRAT) method. RRGMRES applied to the solution of (13) solves at step ℓ the problem

$$\min_{\mathbf{x} \in \mathcal{K}_\ell(M, M\mathbf{b})} \|M\mathbf{x} - \mathbf{b}\|. \quad (25)$$

We use the implementation described in [22]. It is based on the relations

$$MV_\ell = V_{\ell+1}H_{\ell+1,\ell} = V_{\ell+1}Q_{\ell+1,\ell+1}R_{\ell+1,\ell} = W_\ell R_{\ell,\ell}, \quad (26)$$

where the leftmost equality is the Arnoldi decomposition (14) and the next equality follows from (17). Let the matrix $Q_{\ell+1,\ell}$ be made up of the first ℓ columns of $Q_{\ell+1,\ell+1}$ and let $R_{\ell,\ell}$ be the (invertible) leading upper triangular $\ell \times \ell$ submatrix of $R_{\ell+1,\ell}$. Since the latter matrix has a vanishing last row, we have $Q_{\ell+1,\ell+1}R_{\ell+1,\ell} = Q_{\ell+1,\ell}R_{\ell,\ell}$. Letting $W_\ell = V_{\ell+1}Q_{\ell+1,\ell}$ yields the last equality in (26). The columns of W_ℓ are orthonormal. It follows from (26) that they span $\mathcal{K}_\ell(M, M\mathbf{b})$.

We would like to illustrate that the decomposition (26) allows a simple implementation of the discrepancy principle. Express $\mathbf{x} \in \mathcal{K}_\ell(M, M\mathbf{b})$ as $\mathbf{x} = W_\ell \mathbf{y}$. Then

$$\begin{aligned} \|M\mathbf{x} - \mathbf{b}\| &= \|MW_\ell \mathbf{y} - \mathbf{b}\| = \|MV_{\ell+1}Q_{\ell+1,\ell} \mathbf{y} - \mathbf{b}\| \\ &= \|V_{\ell+2}H_{\ell+2,\ell+1}Q_{\ell+1,\ell} \mathbf{y} - \mathbf{b}\| \\ &= \|H_{\ell+2,\ell+1}Q_{\ell+1,\ell} \mathbf{y} - \|\mathbf{b}\| \mathbf{e}_1\| \\ &= \|Q_{\ell+2,\ell+2}R_{\ell+2,\ell+1}Q_{\ell+1,\ell} \mathbf{y} - \|\mathbf{b}\| \mathbf{e}_1\| \\ &= \|R_{\ell+2,\ell+1}Q_{\ell+1,\ell} \mathbf{y} - \|\mathbf{b}\| Q_{\ell+2,\ell+2}^T \mathbf{e}_1\|. \end{aligned}$$

Introduce the QR factorization $R_{\ell+2,\ell+1}Q_{\ell+1,\ell} = \tilde{Q}_{\ell+2,\ell+2}\tilde{R}_{\ell+2,\ell}$, where $\tilde{Q}_{\ell+2,\ell+2} \in \mathbb{R}^{(\ell+2) \times (\ell+2)}$ is orthogonal and $\tilde{R}_{\ell+2,\ell} \in \mathbb{R}^{(\ell+2) \times \ell}$ has a leading $\ell \times \ell$ upper triangular submatrix $\tilde{R}_{\ell,\ell}$ and two vanishing last rows. Substituting this factorization into the last expression above yields

$$\begin{aligned} \min_{\mathbf{x} \in \mathcal{K}_\ell(M, M\mathbf{b})} \|M\mathbf{x} - \mathbf{b}\| &= \min_{\mathbf{y} \in \mathbb{R}^\ell} \|\tilde{Q}_{\ell+2,\ell+2}\tilde{R}_{\ell+2,\ell} \mathbf{y} - \|\mathbf{b}\| Q_{\ell+2,\ell+2}^T \mathbf{e}_1\| \\ &= \min_{\mathbf{y} \in \mathbb{R}^\ell} \|\tilde{R}_{\ell+2,\ell} \mathbf{y} - \|\mathbf{b}\| \tilde{Q}_{\ell+2,\ell+2}^T Q_{\ell+2,\ell+2} \mathbf{e}_1\|. \end{aligned}$$

Writing

$$\|\mathbf{b}\| \tilde{Q}_{\ell+2,\ell+2}^T Q_{\ell+2,\ell+2}^T \mathbf{e}_1 = \begin{bmatrix} \tilde{\mathbf{q}}_\ell \\ \tilde{\mathbf{r}}_\ell \end{bmatrix},$$

with $\tilde{\mathbf{q}}_\ell \in \mathbb{R}^\ell$ and $\tilde{\mathbf{r}}_\ell \in \mathbb{R}^2$, the solution \mathbf{x}_ℓ of (25) can be determined by solving

$$\tilde{R}_{\ell,\ell} \mathbf{y} = \tilde{\mathbf{q}}_\ell$$

for \mathbf{y}_ℓ and computing $\mathbf{x}_\ell = W_\ell \mathbf{y}_\ell$. The residual is given by $\|\tilde{\mathbf{r}}_\ell\|$. Thus the residual norm (25) is available essentially for free. Note that computation of the RRGMRES solution \mathbf{x}_ℓ requires one more step of the Arnoldi process than the corresponding GMRES solution.

When solving either (3) or (7), the value $\|\tilde{\mathbf{r}}_\ell\|$ obtained in the above rendition of RRGMRES is the norm of residual error of (3). We therefore terminate the iterations with RRGMRES as soon as

$$\|\tilde{\mathbf{r}}_\ell\| < \eta \varepsilon \quad (27)$$

holds. Application of the discrepancy principle is more expensive when solving (5). We omit the details.

The range-restricted Arnoldi–Tikhonov (RRAT) method replaces (25) by the penalized least-squares problem

$$\min_{\mathbf{x} \in \mathcal{K}_\ell(M, M\mathbf{b})} \{\|\mathbf{Mx} - \mathbf{b}\|^2 + \mu \|L\mathbf{x}\|^2\}. \quad (28)$$

We let $L = I$. This minimization problem has previously been considered in [20, 22]. It can be solved by setting $\mathbf{x} = W_\ell \mathbf{y}$. Then (28) simplifies to

$$\min_{\mathbf{y} \in \mathbb{R}^\ell} \{\|\tilde{R}_{\ell,\ell} \mathbf{y} - \tilde{\mathbf{q}}_\ell\|^2 + \mu \|\mathbf{y}\|^2\}.$$

This problem can be solved by using a formulation analogous to (23). Denoting the solution by $\mathbf{y}_{\mu,\ell}$, we obtain the associated solution $\mathbf{x}_{\mu,\ell} = W_\ell \mathbf{y}_{\mu,\ell}$ of (28).

When applying the discrepancy principle to either (3) or (7), we seek the solution $\mu = \mu_{\ell,\varepsilon}$ of the equation (in μ)

$$\|\mathbf{Mx}_{\mu,\ell} - \mathbf{b}\| = \eta \varepsilon. \quad (29)$$

We only can determine a solution when ℓ is large enough so that (27) holds.

4 The role of preconditioning

In our applications A is a blurring matrix and, therefore, matrix-vector products with A' can be thought of as a low-pass filter. First consider the situation when the PSF is fairly close to symmetric. Then an advantage of left-preconditioning, as in (5), when compared with the original unpreconditioned system (3), is that high-frequency components of the error $\boldsymbol{\nu}$ in \mathbf{g} typically are damped by the multiplication of \mathbf{g} by A' in the right-hand side. When, instead, solving the right-preconditioned system (7), high-frequency components of the propagated error in the computed solution are damped by requiring the computed solution to be in the range of A' .

In the case of a highly non-symmetric PSF, the advantage of left- and right-preconditioning transcends the damping of high-frequency components. Indeed, in some cases the Krylov subspaces associated with application of GMRES to (5) or (7) provide a fundamentally more relevant basis with which to approximate the original image than the Krylov subspaces associated with (3). When GMRES is applied to the solution of either (5) or (7), the computed approximate solutions determined at step ℓ live in the Krylov subspace

$$\mathcal{K}_\ell(A'A, A'\mathbf{g}) = \text{span} \left\{ A'\mathbf{g}, (A'A)A'\mathbf{g}, \dots, (A'A)^{\ell-1}A'\mathbf{g} \right\}, \quad (30)$$

while ℓ steps of GMRES applied to the solution of (3) computes an approximate solution in the Krylov subspace

$$\mathcal{K}_\ell(A, \mathbf{g}) = \text{span} \left\{ \mathbf{g}, A\mathbf{g}, \dots, A^{\ell-1}\mathbf{g} \right\}. \quad (31)$$

In the case of a highly non-symmetric PSF, such as a PSF modeling motion blur, the vectors in the right-hand side of (31) tend to represent images that drift away spatially from the original image. The vectors in the right-hand side of (30), on the other hand, tend to represent increasingly blurred images which are centered at roughly the correct place. The reason for this is that each multiplication by A is followed by a multiplication by A' , and the latter models motion blur in the direction opposite to that of A .

The following example illustrates this discussion. Convolution of the sharp image represented by \mathbf{f} of Figure 2 with the highly nonsymmetric motion PSF of Figure 1 yields the blurred image \mathbf{g} . The first four basis vectors of the Krylov subspaces (31) and (30) are displayed by the images 2 through 5 of rows 1 and 2 in Figure 2, respectively. The final image of row 1 corresponds to the optimal (minimum Euclidean norm error) solution when applying GMRES to (3). This solution is attained already at iteration 1. The final image of row 2 corresponds to the optimal solution when applying GMRES to (7). It is attained at iteration 82. Notice that the latter restoration is far superior to the former. When applying GMRES to (3), only the first basis image is of any use for approximating \mathbf{f} ; subsequent basis images drift towards the bottom-right corner of the domain.

5 Numerical examples

We compare for four image restoration problems with ARBC the performance of the methods discussed in Section 3 to that of the CGLS-based approach of [9]. All numerical experiments are conducted in MATLAB R2011a with $\epsilon_{\text{machine}} = 2.22 \times 10^{-16}$. The blurring operators A are represented as a `psfMatrix` object from the MATLAB package `RestoreTools` [21]. Each corrupted image \mathbf{g} is produced by first applying the appropriate blurring operator to an original sharp image, and then extracting an interior image to ensure realistic contributions from pixels outside the FOV. This yields a blurred image $\tilde{\mathbf{g}}$. Next white Gaussian noise $\boldsymbol{\nu}$ of relative norm

$$\sigma = \frac{\|\boldsymbol{\nu}\|}{\|\tilde{\mathbf{g}}\|},$$

is added to $\tilde{\mathbf{g}}$ to obtain \mathbf{g} . In the original figures, the FOV is marked by a black or white box.

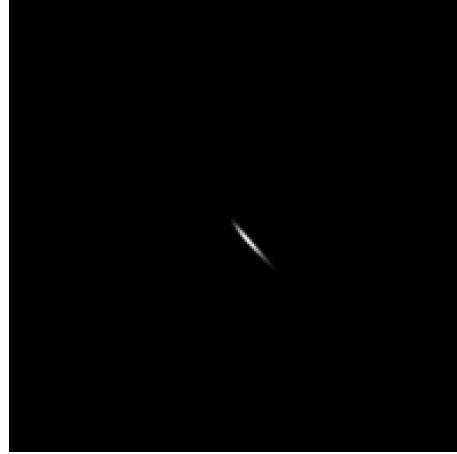


Figure 1: A PSF (29×29) modelling motion blur.

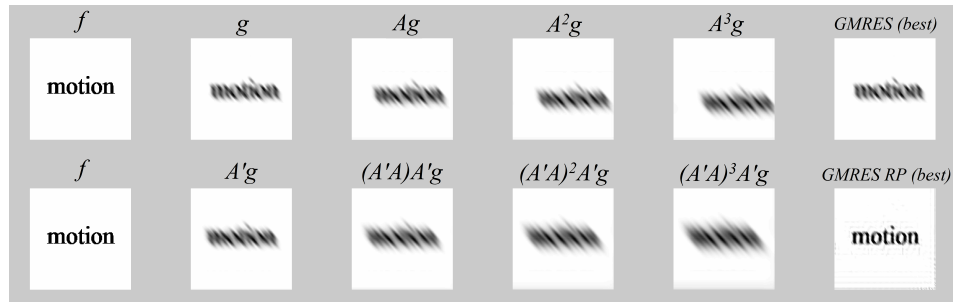


Figure 2: Row 1: the sharp image f , the first four basis images of the Krylov subspace (31), and the optimal solution when applying GMRES to (3). Row 2: the sharp image f , the first four basis images of the Krylov subspace (30), and the optimal solution when applying GMRES to (7).

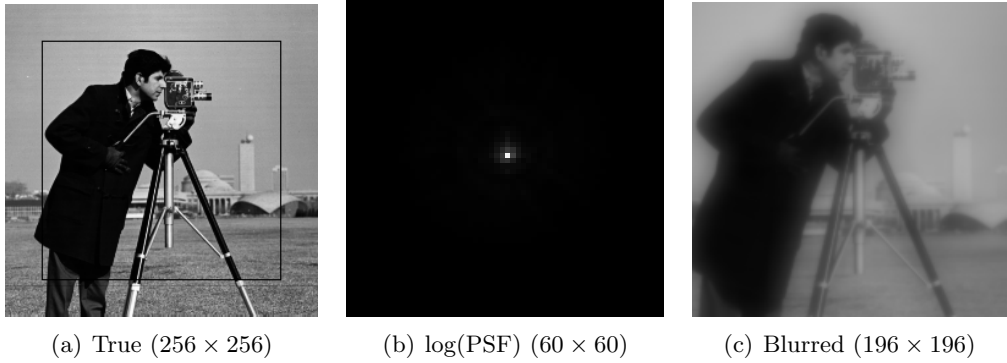


Figure 3: Example 1: true 256×256 cameraman image with FOV, PSF in logarithmic scale, and blurred image.

The accuracy of the restorations is measured by the peak signal-to-noise ratio (PSNR), defined by

$$\text{PSNR} = 10 \log_{10} \frac{n^2}{\|\tilde{\mathbf{f}} - \mathbf{f}\|^2},$$

where $\tilde{\mathbf{f}}$ is a restoration of the true image \mathbf{f} . Here $\|\cdot\|$ is the Euclidean vector norm and the $n \times n$ images are represented by vectors of size n^2 . A large PSNR-value generally indicates that the restoration is of high quality.

Throughout this section we apply the discrepancy principle (21) with $\eta = 1$. It is possible that for some examples, in particular when the matrix A is decidedly nonsymmetric, better restorations may be achieved by choosing $\eta > 1$ appropriately. However, it is difficult to choose an appropriate value for η in an automatic way without user interaction. We therefore set $\eta = 1$ in all computations. To gain some insight into how a different choice of η may affect the quality of the computed restoration, we also report PSNR-values for the best restorations that can be determined by the methods, i.e., the restorations with the largest PSNR-value, within 100 iterations.

For Tikhonov regularization, we determine the regularization parameter so that the discrepancy principle (24) or (29) with $\eta = 1$ are satisfied and report results achieved both for the minimum number of iterations that allows the discrepancy principle to be satisfied and for the number of iterations that gives a restoration with the largest PSNR-value.

We compare right-preconditioning (RP) and left-preconditioning (LP) strategies for methods based on the Arnoldi process to CGLS applied to the solution of (5); the latter iterative method is obtained by replacing the matrix A^T by A' in the recursion formulas for the standard CGLS method. First we consider a nonsymmetric PSF that is close to quadrantly symmetric to illustrate that, at least for small noise levels σ , CGLS and range restricted Arnoldi methods can provide accurate restorations.

Example 1. We seek to restore a cameraman image that has been contaminated by blur and noise. The blur is defined by a nonsymmetric PSF, that is close to quadrantly symmetric. Figure 3 shows the true image (within the FOV), the PSF, and the blurred image without noise.

Method	$\sigma = 0.01$		$\sigma = 0.05$	
	max PSNR (it.)	stop PSNR (it.)	max PSNR (it.)	stop PSNR (it.)
CGLS	27.07 (15)	26.58 (12)	21.54 (5)	21.54 (5)
GMRES	26.48 (5)	26.48 (5)	20.09 (2)	18.11 (13)
RRGMRES	26.92 (8)	26.68 (7)	21.70 (4)	21.70 (4)
GMRES LP	27.19 (19)	26.57 (15)	22.04 (8)	21.71 (6)
GMRES RP	27.09 (15)	26.75 (13)	21.98 (6)	21.98 (6)
RRGMRES LP	27.23 (34)	26.54 (27)	22.46 (16)	22.13 (13)
RRGMRES RP	27.03 (29)	26.55 (25)	22.31 (14)	22.18 (12)
AT	26.52 (29)	26.51 (13)	20.93 (14)	20.93 (14)
RRAT	26.72 (9)	26.54 (15)	21.60 (4)	20.91 (11)
AT LP	26.47 (48)	26.36 (18)	22.04 (21)	21.60 (9)
AT RP	26.46 (46)	26.35 (17)	22.03 (30)	22.03 (19)

Table 1: Example 1: PNSR-values with the corresponding iteration number in brackets for the restoration with maximum PSNR and for the restoration determined when terminating the iterations with the discrepancy principle. Results for the noise levels $\sigma = 0.01$ and $\sigma = 0.05$ are presented. The largest entry in each column is in boldface.

We consider both a moderate noise level with $\sigma = 0.01$, and a larger one with $\sigma = 0.05$. Table 1 shows PSNR-values of the restorations determined by iterative methods when the iterations are terminated by the discrepancy principle. Table 1 shows that for $\sigma = 0.01$ both CGLS and RRGMRES applied to (3) determine restorations of about the same quality as obtained with preconditioning, but when $\sigma = 0.05$ right-preconditioning helps to improve the quality of the restoration. This is confirmed by visual perception; see Figures 4-5.

Example 2. The boat image of Figure 6 is contaminated by motion blur and noise. Table 2 shows the discrepancy principle to fail for the CGLS, GMRES, and RRGMRES iterative methods

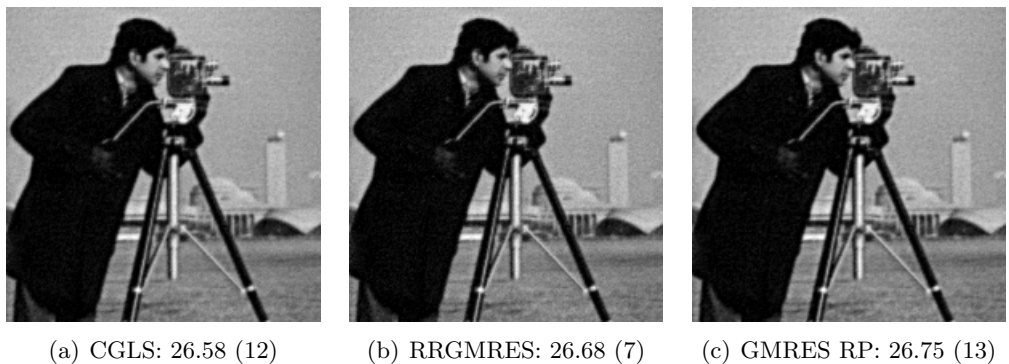


Figure 4: Example 1: Restored images determined with the discrepancy principle for $\sigma = 0.01$. The PSNR-value and number of iterations are reported for each method.

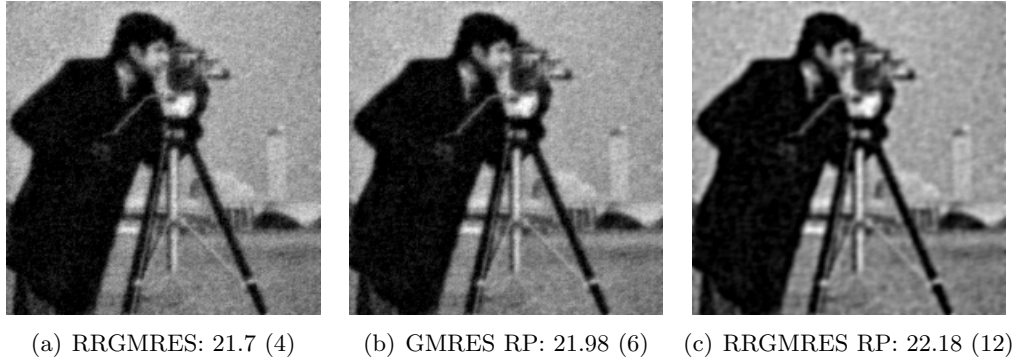


Figure 5: Example 1: Restored images determined with the discrepancy principle for $\sigma = 0.05$. The PSNR-value and number of iterations are reported for each method.

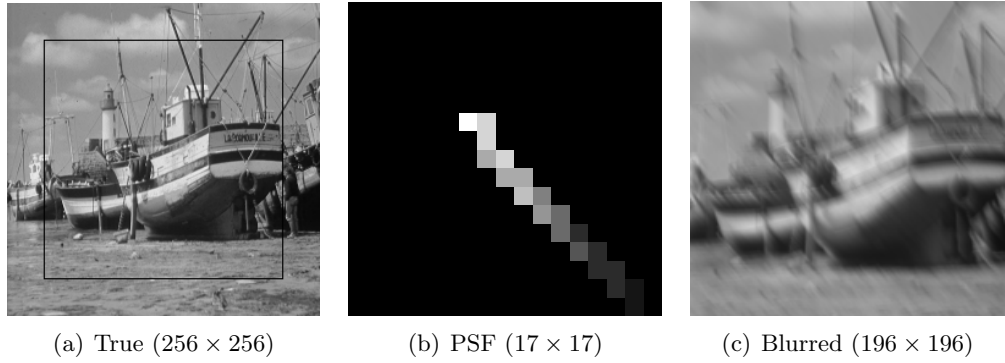


Figure 6: Example 2: true 256×256 boat image with FOV, PSF, and blurred image.

when a low level of noise is present. Nevertheless, the restored image determined by GMRES with reblurring right preconditioner and termination with the discrepancy principle, shown in Figure 7, is of higher quality than the restorations with maximum PSNR-values computed by CGLS and GMRES.

Example 3. We contaminate the **peppers** image by motion blur in two directions as well as by noise; see Figure 9. Standard methods based on the Arnoldi process do not perform well for this difficult deconvolution problem, and neither does CGLS; see Table 3. On the other hand, the right-preconditioned methods perform well for different noise levels, even though some “ringing” effects are visible at the right boundary of the restored images; see Figures 10–11.

Example 4. In this last example, we consider an astronomical deconvolution problem. The **Saturn** image in Figure 12 is distorted by atmospheric blur from the **RestoreTools 2.0** toolbox and considerable noise ($\sigma = 0.03$ and $\sigma = 0.07$).

The PSNR-values of the restored images are reported in Table 4. Note that for this example RRGMRES and range restricted Arnoldi-based Tikhonov regularization yield restorations of much higher quality than GMRES and standard Arnoldi-based Tikhonov regularization, even

Method	$\sigma = 0.005$		$\sigma = 0.03$	
	max PSNR (it.)	stop PSNR (it.)	max PSNR (it.)	stop PSNR (it.)
CGLS	28.65 (12)	#	24.60 (5)	24.60 (5)
GMRES	25.63 (15)	#	20.96 (4)	18.97 (11)
RRGMRES	21.70 (22)	#	19.33 (11)	#
GMRES LP	31.68 (25)	30.90 (17)	25.09 (7)	24.79 (5)
GMRES RP	31.55 (22)	31.14 (16)	24.96 (6)	24.95 (5)
RRGMRES LP	31.36 (45)	30.50 (31)	24.78 (15)	24.51 (11)
RRGMRES RP	31.27 (42)	30.63 (30)	24.62 (12)	24.56 (11)
AT	25.63 (15)	#	20.96 (4)	19.28 (17)
RRAT	21.71 (22)	#	19.33 (11)	#
AT LP	30.90 (25)	30.88 (21)	24.72 (7)	24.72 (8)
AT RP	30.92 (15)	30.87 (20)	24.67 (6)	24.62 (17)

Table 2: Example 2: PNSR-values with the corresponding iteration number in brackets for the restoration with maximum PSNR and for the restoration determined when terminating the iterations with the discrepancy principle. Results for the noise levels $\sigma = 0.005$ and $\sigma = 0.03$ are presented. The symbol # indicates that the discrepancy principle is never satisfied.

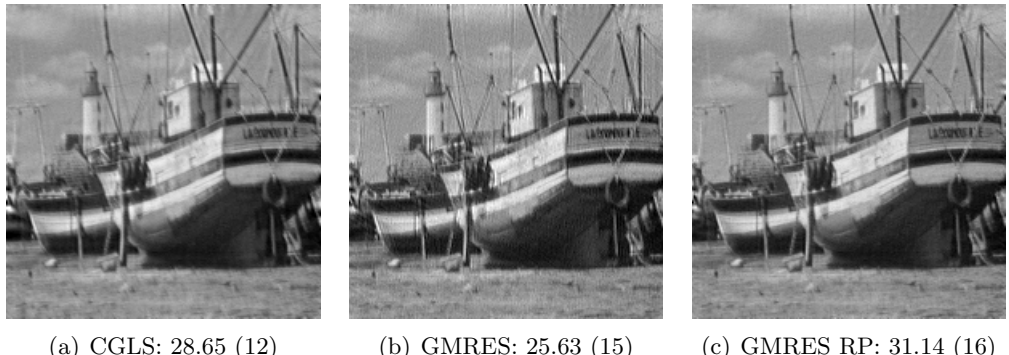


Figure 7: Example 2: Restored images with maximal PSNR-values computed by CLGS and GMRES, and the restoration determined by GMRES RP with the iterations terminated by the discrepancy principle. The noise level is $\sigma = 0.005$. PSNR-values and the number of iterations are reported for each method.

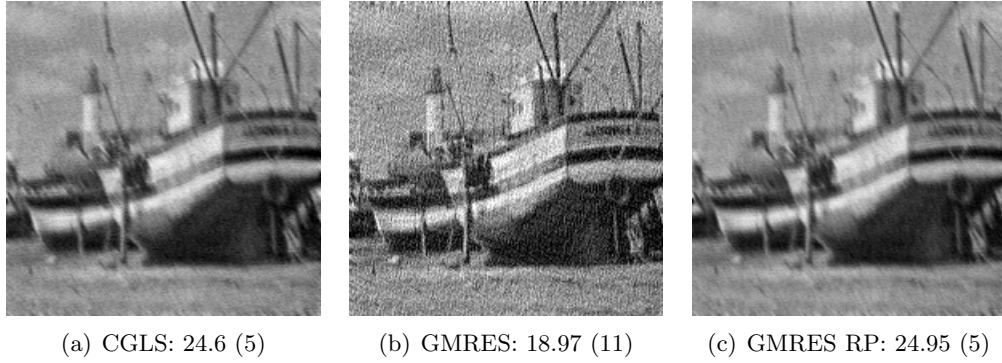


Figure 8: Example 2: Restored images determined with the discrepancy principle. The noise level is $\sigma = 0.03$. PSNR-values and the number of iterations are reported for each method.

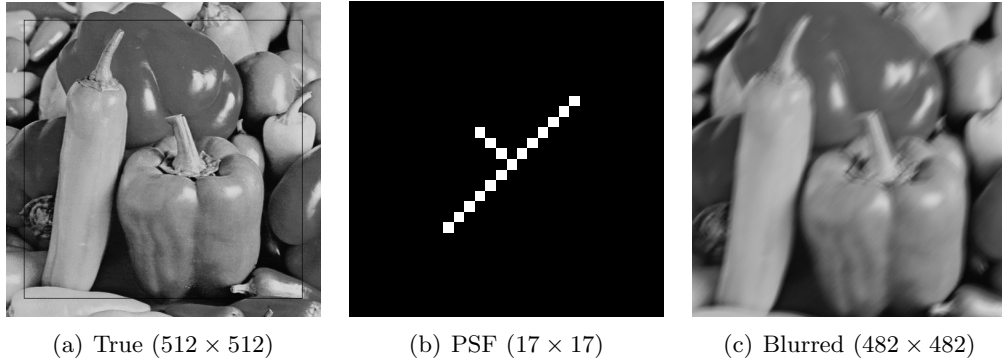


Figure 9: Example 3: The true 512×512 peppers image with FOV, the PSF, and the blurred image.

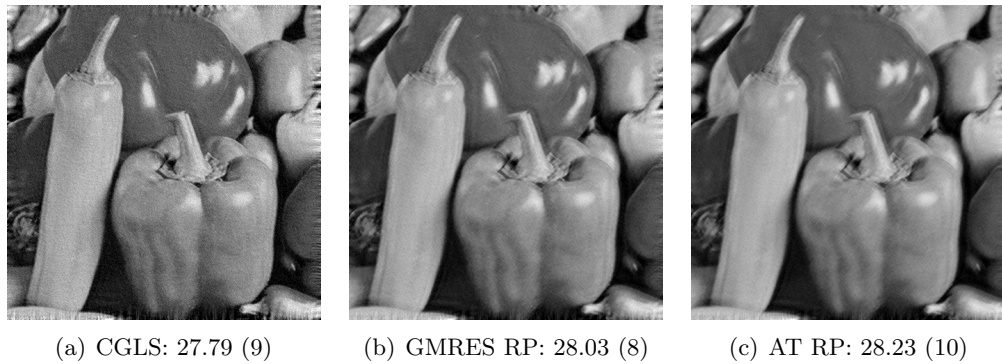


Figure 10: Example 3: Restored images with maximum PSNR-values determined by CLGS and restorations determined by GMRES RP and AT RP using the discrepancy principle. The noise level is $\sigma = 0.02$. The PSNR-values and the number of iterations are reported for each method.

Method	$\sigma = 0.02$		$\sigma = 0.06$	
	max PSNR (it.)	stop PSNR (it.)	max PSNR (it.)	stop PSNR (it.)
CGLS	27.79 (9)	#	24.76 (4)	24.76 (4)
GMRES	18.46 (90)	#	18.09 (84)	#
RRGMRES	16.04 (84)	#	15.98 (83)	#
GMRES LP	28.20 (7)	28.13 (8)	26.19 (3)	26.19 (3)
GMRES RP	28.17 (6)	28.03 (8)	26.10 (3)	26.10 (3)
RRGMRES LP	27.69 (14)	#	26.05 (7)	26.03 (6)
RRGMRES RP	27.79 (15)	27.53 (23)	26.01 (6)	26.01 (11)
AT	18.46 (90)	#	18.09 (84)	#
RRAT	16.04 (84)	#	15.98 (83)	#
AT LP	28.23 (10)	28.23 (11)	26.12 (18)	26.11 (10)
AT RP	28.23 (10)	28.23 (10)	26.10 (11)	26.10 (11)

Table 3: Example 3: PNSR-values with the corresponding iteration number in brackets for the restoration with maximum PSNR and for the restoration determined when terminating the iterations with the discrepancy principle. Results for the noise levels $\sigma = 0.02$ and $\sigma = 0.06$ are presented. The symbol # indicates that the discrepancy principle is never satisfied.

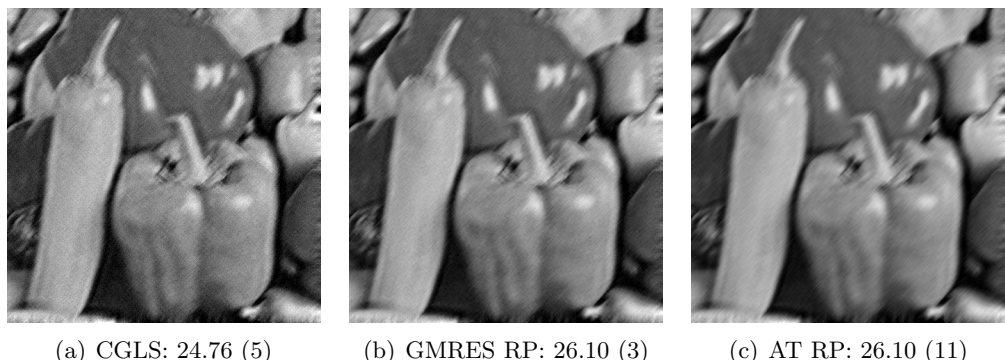


Figure 11: Example 3: Restored images using the discrepancy principle. The noise level is $\sigma = 0.06$. The PSNR-values and number of iterations are reported for each method.

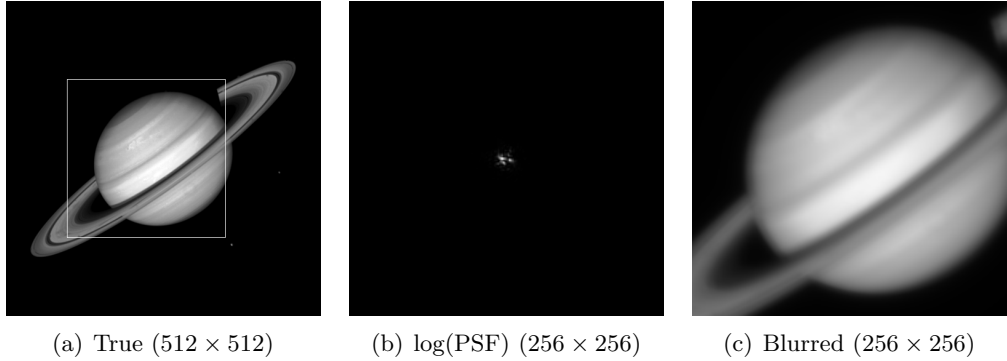


Figure 12: Example 4: true 256×256 Saturn image with FOV, PSF in logarithmic scale, and blurred image.

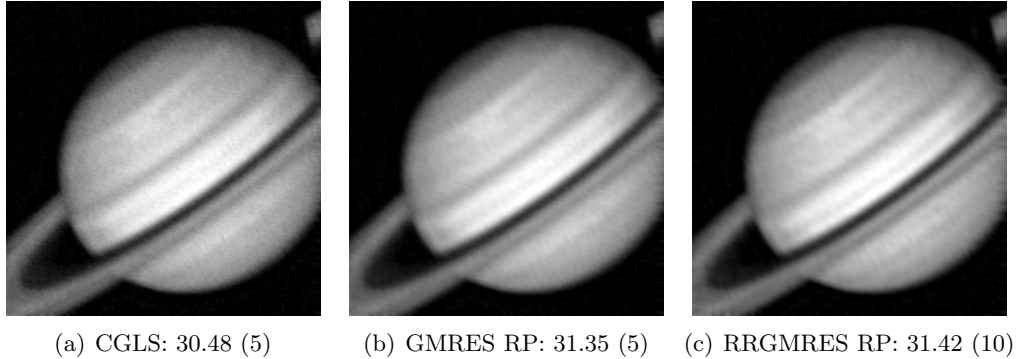


Figure 13: Example 4: Restored images using the discrepancy principle. The noise level is $\sigma = 0.03$. The PSNR-values and number of iterations are reported for each method.

though the discrepancy principle fails for $\sigma = 0.03$. Range restricted methods do not deliver improved restorations when right-preconditioning is used in the case of $\sigma = 0.03$; see also Figure 13. For $\sigma = 0.07$, Figure 14 shows that it may be beneficial to combine right reblurring preconditioning with range restricted methods.

6 Conclusion

We have compared the performance of iterative methods and Tikhonov regularization with right and left preconditioning when applied to the restoration of images that have been contaminated by blur defined by a nonsymmetric PSF, and ARBC are imposed. The proposed techniques can be applied also to RBC, synthetic BC (see [15]), and other models for which the matrix A^T is not available or is difficult to use.

A theoretical justification in terms of the effect of using different Krylov subspaces is provided and a large number of computed examples support our proposal to apply methods based on the Arnoldi process with a right reblurring preconditioner A' . Our numerical results show this kind of solution methods to be robust for all noise levels and for a variety of PSFs. The iterations

Method	$\sigma = 0.03$		$\sigma = 0.07$	
	max PSNR (it.)	stop PSNR (it.)	max PSNR (it.)	stop PSNR (it.)
CGLS	30.48 (5)	30.48 (5)	26.69 (3)	26.69 (3)
GMRES	27.29 (2)	24.51 (3)	24.54 (1)	21.78 (2)
RRGMRES	30.14 (4)	#	28.45 (3)	26.11 (5)
GMRES LP	31.40 (6)	31.21 (5)	29.71 (4)	29.71 (4)
GMRES RP	31.35 (5)	31.35 (5)	29.51 (4)	29.51 (4)
RRGMRES LP	31.47 (11)	31.37 (10)	30.20 (8)	30.05 (7)
RRGMRES RP	31.42 (10)	31.42 (10)	30.11 (7)	30.11 (7)
AT	27.52 (100)	27.04 (8)	25.65 (100)	25.57 (15)
RRAT	30.14 (4)	#	28.45 (3)	26.75 (14)
AT LP	31.36 (14)	31.21 (8)	29.95 (34)	29.94 (12)
AT RP	31.37 (43)	31.18 (6)	30.02 (38)	29.99 (12)

Table 4: Example 4: PNSR-values with the corresponding iteration number in brackets for the restoration with maximum PSNR (within 100 iterations) and for the restoration determined when terminating the iterations with the discrepancy principle. Results for the noise levels $\sigma = 0.03$ and $\sigma = 0.07$ are displayed. The symbol # indicates that the discrepancy principle is never satisfied.

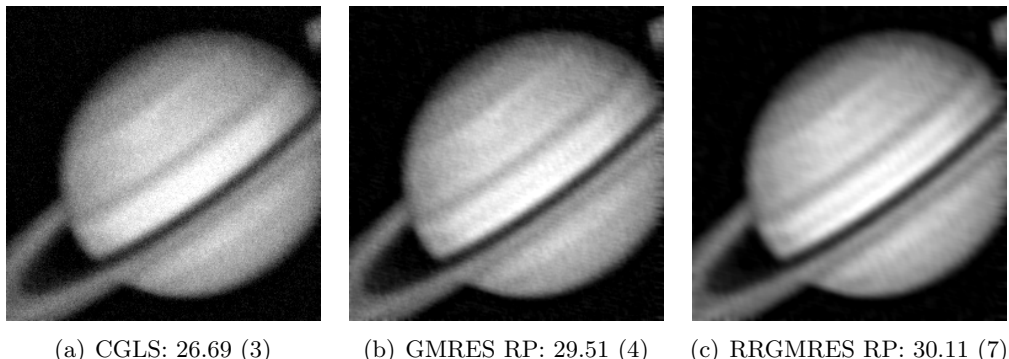


Figure 14: Example 4: Restored images using the discrepancy principle. The noise level is $\sigma = 0.07$. The PSNR-values and number of iterations are reported for each method.

can be terminated by the discrepancy principle with no additional cost, since the norm of the residual vector is available for free in the Arnoldi process. Range restricted methods generally do not yield improved restorations when right-preconditioning is used, at least for images with fairly little noise-contamination.

Acknowledgment

We would like to thank Giuseppe Rodriguez and the referees for carefully reading a previous version of this paper and for suggestions that improved the presentation. The work of the first author is partly supported by PRIN 2012 N. 2012MTE38N and the work of the second and third authors is supported in part by NSF grant DMS-1115385.

References

- [1] A. Aricò, M. Donatelli, J. Nagy, and S. Serra–Capizzano, *The anti-reflective transform and regularization by filtering*, in Numerical Linear Algebra in Signals, Systems, and Control, Lecture Notes in Electrical Engineering, vol. 80, Springer, 2011, pp. 1–21.
- [2] A. Aricò, M. Donatelli, and S. Serra–Capizzano, *Spectral analysis of the anti-reflective algebra*, Linear Algebra Appl., 428 (2008), pp. 657–675.
- [3] M. Bertero and P. Boccacci, *Introduction to Inverse Problems in Imaging*, Inst. of Physics Publ., Bristol, 1998.
- [4] M. Bertero and P. Boccacci, *A simple method for the reduction of the boundary effects in the Richardson–Lucy approach to image deconvolution*, Astron. Astrophys., 437 (2005), pp. 369–374.
- [5] Å. Björck, *Numerical Methods for Least Squares Problems*, SIAM, Philadelphia, 1996.
- [6] D. Calvetti, B. Lewis, and L. Reichel, *On the regularizing properties of the GMRES method*, Numer. Math., 91 (2002), pp. 605–625.
- [7] D. Calvetti, S. Morigi, L. Reichel, and F. Sgallari, *Tikhonov regularization and the L-curve for large, discrete ill-posed problems*, J. Comput. Appl. Math., 123 (2000), pp. 423–446.
- [8] M. Christiansen and M. Hanke, *Deblurring methods using antireflective boundary conditions*, SIAM J. Sci. Comput., 30 (2008), pp. 855–872.
- [9] M. Donatelli, C. Estatico, A. Martinelli, and S. Serra–Capizzano, *Improved image deblurring with anti-reflective boundary conditions and re-blurring*, Inverse Problems, 22 (2006), pp. 2035–2053.
- [10] M. Donatelli and M. Hanke, *On the condition number of the antireflective transform*, Linear Algebra Appl., 432 (2010), pp. 1772–1784.
- [11] M. Donatelli and S. Serra–Capizzano, *Anti-reflective boundary conditions and re-blurring*, Inverse Problems, 21 (2005), pp. 169–182.

- [12] M. Donatelli and S. Serra–Capizzano, *Anti-reflective boundary conditions for deblurring problems*, Journal of Electrical and Computer Engineering, vol. 2010 (2010), Article ID 241467, 18 pages.
- [13] M. Donatelli, C. Estatico, J. Nagy, L. Perrone, and S. Serra–Capizzano, *Anti-reflective boundary conditions and fast 2D deblurring models*, in Advanced Signal Processing Algorithms, Architectures, and Implementations XIII, ed. F. T. Luk, Proc. SPIE, vol. 5205, 2003, pp. 380–389.
- [14] H. W. Engl, M. Hanke, and A. Neubauer, *Regularization of Inverse Problems*, Kluwer, Dordrecht, 1996.
- [15] J. W. Fan and J. G. Nagy, *Synthetic boundary conditions for image deblurring*, Linear Algebra Appl., 434 (2011) 2244–2268.
- [16] S. Gazzola, *Regularization techniques based on Krylov subspace methods for ill-posed linear systems*, Ph.D. thesis, Department of Mathematics, University of Padova, Padova, Italy, 2013.
- [17] S. Gazzola and P. Novati, *Automatic parameter setting for Arnoldi–Tikhonov methods*, J. Comput. Appl. Math., 256 (2014), pp 180–195.
- [18] T. A. Hearn and L. Reichel, *Extensions of the Justen–Ramlau blind deconvolution method*, Adv. Comput. Math., 39 (2013), pp. 465–491.
- [19] M. E. Hochstenbach, N. McNinch, and L. Reichel, *Discrete ill-posed least-squares problems with a solution norm constraint*, Linear Algebra Appl., 436 (2012), pp. 3801–3818.
- [20] B. Lewis and L. Reichel, *Arnoldi–Tikhonov regularization methods*, J. Comput. Appl. Math., 226 (2009), pp. 92–102.
- [21] J. Nagy, K. Palmer, and L. Perrone, *RestoreTools: an object oriented MATLAB package for image restoration*, 2002, <http://www.mathcs.emory.edu/~nagy/RestoreTools/>.
- [22] A. Neuman, L. Reichel, and H. Sadok, *Implementations of range restricted iterative methods for linear discrete ill-posed problems*, Linear Algebra Appl., 436 (2012), pp. 3974–3990.
- [23] M. Ng, R. H. Chan, and W. C. Tang, *A fast algorithm for deblurring models with Neumann boundary conditions*, SIAM J. Sci. Comput., 21 (1999) pp. 851–866.
- [24] L. Reichel, F. Sgallari, and Q. Ye, *Tikhonov regularization based on generalized Krylov subspace methods*, Appl. Numer. Math., 62 (2012), pp. 1215–1228.
- [25] L. Reichel and X. Yu, *Tikhonov regularization via flexible Arnoldi reduction*, BIT Numer. Math., in press.
- [26] Y. Saad and M. H. Schulz, *GMRES: A generalized minimal residual method for solving nonsymmetric linear systems*, SIAM J. Sci. Stat. Comput., 7 (1986), pp. 856–869.

- [27] S. Serra-Capizzano, *A note on anti-reflective boundary conditions and fast deblurring models*, SIAM J. Sci. Comput., 25 (2003), pp. 1307–1325.
- [28] R. Vio, J. Bardsley, M. Donatelli, and W. Wamsteker, *Dealing with edge effects in least-squares image deconvolution problems*, Astron. Astrophys., 442 (2005), pp. 397–403.